Journal of Ultrafine Grained and Nanostructured Materials
https://jufgnsm.ut.ac.ir
Vol. 54, No.1, June 2021, pp. 85-92
Print ISSN: 2423-6845 Online ISSN: 2423-6837
DOI: 10.22059/jufgnsm.2021.01.09

Effect of cathode size on the morphology of the anodized TiO2 nanotube photocatalyst

Elham Montakhab, Fereshteh Rashchi*, Saeed Sheibani

School of Metallurgy and Materials Engineering, College of Engineering, University of Tehran, Tehran, Iran.

Recieved: 20 November 2020; Accepted: 18 December 2020
** Corresponding author email: rashchi@ut.ac.ir*

ABSTRACT

Titanium dioxide nanotubes (TNTs) were synthesized via an electrochemical anodization process. The influence of increasing the cathode surface area on the microstructure and order of the final product was investigated. To study the microstructure of the synthesized nanotubes, field emission scanning electron microscopy (FESEM) was employed. The degree of crystallinity and the characteristic of synthesized nanostructure was evaluated by X-ray diffraction (XRD). The porous initiation layer covering the tube-top became thinner and lost its' integrity, as a consequence of employing a larger cathode. This is due to the enhanced reaction sites followed by intensifying the electrochemical reaction in the anodic oxidation processes. In contrast, a small surface area of the cathode made it possible to control the obtained nanostructure with no damages to the surface morphology. The average diameter of the surface nanopores increased from 60 to 67 nm by increasing the cathode surface area. Optical characterization demonstrates that the bandgap of the synthesized TiO_2 nanotubes is about 3.2 eV. In the process of methylene blue (MB) degradation, the photocatalytic activity of the TNTs with an ordered initiation layer reaches 69% after 480 min irradiation.

Keywords: *Anodization, TiO_2 nanotubes, Cathode surface area, Photocatalyst.*

1. Introduction

Titanium dioxide is a widely used semiconductor because of its nontoxicity, photo-stability, and relatively low cost possessing favorable physical, optical and electrical properties. Therefore, TiO_2, is one of the most promising materials for use in photocatalysis, dye-sensitized solar cells, gas sensors, and biomedical devices [1]. Nevertheless, the wide bandgap of TiO_2 (3.2 eV for anatase) limits its absorption in the UV irradiation. Moreover, the fast recombination of the charge carriers greatly lowers the photonic efficiency and mainly limit photocatalytic application [2,3]. Therefore, intense efforts focus on modifying the electronic properties of TiO_2 by bandgap engineering, doping, or by suitable modification of the TiO_2 surface (sensitization or junction formation) [4-7]. Not only the material but also its structure and morphology can have considerable impact on the photocatalytic performance. Nanoparticles of TiO_2 in suspend system encountered three vital technical problems (the need for separation, particles aggregation). To avoid these problems various methods have been developed to prepare TiO_2 films on solid support, despite lower efficiency of immobilized system [8]. It is believed that fabrication of TiO_2 in the form of nanostructure such as nanotube, nanowire, and nanobelt can effectively enhance the catalytic

properties of TiO_2 [3,9]. Among them, a great attention has been focused on the titanium dioxide nanotubes (TNTs) due to their larger specific surface areas (30-50 m^2/g) and superior electron transport properties [10-12].

Up to now, three main paths have been established to fabricate TiO_2 nanotubes, via a template-based method, hydrothermal synthesis, and anodization. Among them, the anodization method can make highly ordered TiO_2 arrays immobilized on titanium with good uniformity and capability of massive production [12,13]. The synthesis of TNTs via electrochemical anodization was first reported by Zwilling et al in 1999. Larger specific surface area and superior electron transport properties are some of the unique features of TNTs [11,12]. Anodization conditions can affect the surface morphology, chemical composition, and photocatalytic properties of TNTs [13]. Different tube-top morphology could be appeared during anodization, including a well-defined open mouth, covered with an initiation layer, or a grassy layer [14,15]. Therefore, the accessible surface area could be determined by tube-top morphology, which can significantly affect the photocatalytic efficiency. Many authors have investigated the effect of electrolyte composition and pH on the TNTs properties. Moreover, the effect of the cathode material used in the anodization process was also investigated and some materials such as Fe, Co, Pd, and C showed promising results so as to replace the conventionally used Pt cathode. However, to the knowledge of the authors, the effect of the cathode surface area has not yet been widely explored in the TNT structures [16,17]. In this paper, TiO_2 nanotubes were synthesized via a facile electrochemical anodization method. The effect of the surface area ratio of the cathode to the anode was investigated on the final surface morphology of the anodized samples. The photocatalytic performance of the synthesized TNTs in degradation of an organic pollutant was evaluated.

2. Materials and methods

2.1. Synthesis

Titanium samples with dimensions of 10×30×0.5 mm were cut from a Ti plate (thickness 0.5 mm, purity >99.6%). Before anodization, the Ti samples were ground with SiC paper from P320 to P3000. They were cleaned by sonication in acetone, isopropanol, and ethanol for 15 minutes. Then, the samples were rinsed thoroughly with distilled water and dried in the air. As illustrated in Fig. 1, anodization was conducted in a two-electrode cell configuration connected to a direct current (DC) power supply, where graphite served as the counter electrode (cathode) and the Ti as the anode.

The anodizing area of the Ti sheet was maintained constant (~ 1 cm^2), while two different sizes of graphite (~ 2 and 6 cm^2) were employed. Therefore, the surface area ratio of the cathode to the anode was increased from 2 to 6, and the corresponding samples name was TNT-2 and TNT-6, respectively. The electrolyte was ethylene glycol containing 0.3 wt% NH_4F and 2 vol% H_2O. The samples were anodized for 75 minutes at a constant applied potential of 30 V and all experiments were carried out at room temperature with stirring of the electrolyte. The nanotube layer was then peeled-off by ultrasonication. The detachment of the TNTs could act as an electro-polishing process for the second step. It is worth to mention that, the

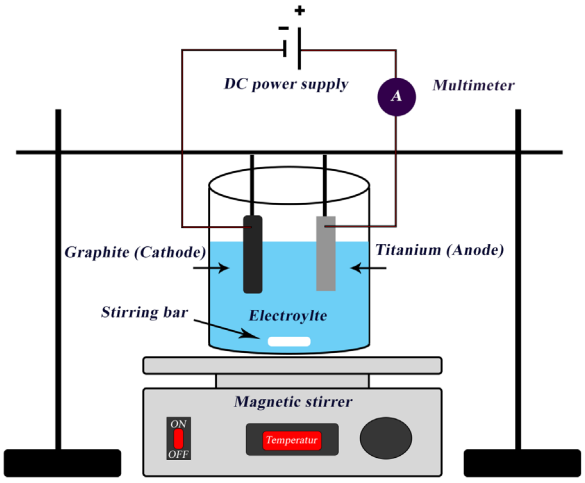

Fig. 1- Schematic diagram of the anodization set-up.

smaller cathode size was used in the first step of anodization and the cathode size was just altered for the second step of anodization. The samples were then anodized for the second time in the same electrolyte with the same conditions but different cathode size. Finally, the samples were rinsed thoroughly with distilled water and dried in the air. Since the as-anodized TNTs are amorphous, they were subsequently heat-treated at 450 °C for different time to define the duration in which complete conversion to anatase phase is obtained with no trace of rutile (with the heating and cooling rate of 5 °C/min).

2.2. Characterization

The degree of crystallinity and the characteristic of synthesized structures were evaluated by X-ray diffraction (PANalytical/X'pert PRO) using Cu Kα (λ=0.154 nm). The morphology of the synthesized films was studied by the FESEM (CamScan MV2300, Czech & England). The UV-vis diffuse reflectance spectroscopy (Avaspec 2048 TSC, The Netherlands) was used to estimate the bandgap energy (E_g). The Kubelka-Munk function, F(R), shows the optical absorbance of the synthesized TNTs to be approximated from its reflectance. The Kubelka-Munk is given by the following equation:

$$F(R) = \frac{(1-R)^2}{2R} \quad (1)$$

where R is the reflectance. The bandgap was calculated from the plot of the modified Kubelka-Munk function, $(F(R)h\nu)^{0.5}$ vs energy of the absorbed light [18].

2.3. photocatalytic activity

The photocatalytic activity of the synthesized TiO_2 nanotubes was evaluated by the photodegradation of a 2 mgL^{-1} aqueous solution of methylene blue (MB). The effective surface area of the sample was measured to be 1 cm^2. The distance between the light source and the solution was about 10 cm. The solution was magnetic stirred in the dark for 30 minutes to reach absorption/desorption equilibrium. It was then irradiated at room temperature under UV light illumination (wavelength of 365 nm and power of 0.6 mW cm^{-2}). The UV-light intensity was measured by UVA radiometer (CHY 732, Taiwan). Eventually, the concentration of the remaining MB was determined by UV-vis spectrophotometer (Shimadzu, UVmini 1240, Japan).

3. Results and discussion

3.1. Characterization results

Fig. 2 shows the XRD patterns of the as-prepared and annealed TNT-2 sample. The crystallization of TiO_2 nanotubes at 450 °C allows us to obtain a high anatase content with no rutile peak. The anatase phase benefits from better photocatalytic activities due to higher electron mobility compared to rutile [15,19]. The as-prepared TNTs are amorphous and by following thermal treatment this amorphous phase is converted to the anatase. The low-intensity peak at about 30° belongs to the organic compound on the sample without annealing and annealed for a shorter time [20]. To find adequate annealing time which ensures a complete conversion, two different duration (120 and 180 min) were explored [21-23].

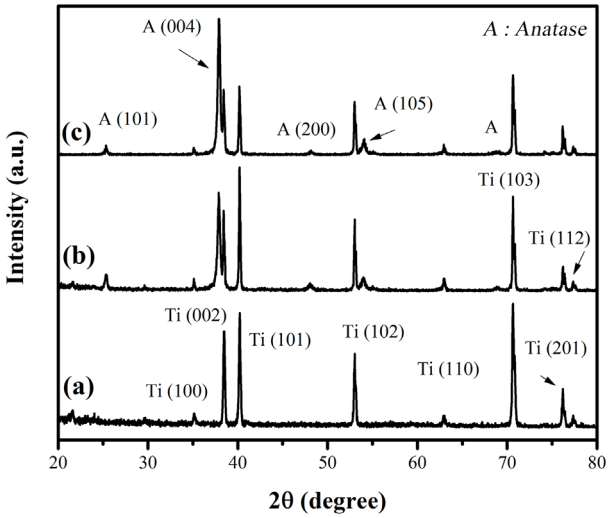

Fig. 2- XRD patterns of the synthesized TNT (a) the as-prepared, (b) as annealed at 450 °C for 120, and (c) 180 minutes.

Both XRD patterns for annealed sample in Fig. 2 confirm the presence of anatase phase as the single-phase in synthesized TNTs beside Ti metal peaks which belongs to the substrate. The background noise in the sample annealed for 120 min, indicates that full conversion to the anatase phase requires longer time. By extending the duration of the annealing to 180 min, diminished background noise implies the full conversion.

Fig. 3 shows the nanotube morphology for various cathode sizes. Both samples in this figure represent a thin porous initiation layer which has been located on the top of the nanotubes. The integrity of the initiation layer has been lost by using the cathode with a larger size (Fig. 3a). While Fig. 3b demonstrate the surface morphology of the TNT-2 sample. An ordered thin porous initiation layer with complete integrity was observed for this sample. As the cathode surface area increases the amount of TiO_2 on the initiation layer is reduced due to the chemical etching by the fluoride ions, which is discussed further [15,20,24]. These morphological features, as discussed in our previous research [15], demonstrate to have a strong impact on the photocatalytic activities of the synthesized TiO_2 nanotubes [15]. The average diameter of the surface nanopores for TNT-2 and TNT-6 are ~ 60 ± 2 and 67 ± 3 nm, respectively. By increasing the surface area of the cathode, the thickness of the synthesized TNTs grew from 3.5 ± 0.2 to 3.9 ± 0.2 μm.

TiO_2 nanotubes array was produced as a result of electrochemical etching of titanium in the presence of fluoride ions. Often, electrochemical reactions, such as anodization processes, are characterized by current-time curves (Fig. 4). The current-time curves show the typical curve for a condition that leads to nanotubes formation. The I-t curve consists of three stages: I) the formation of a compact titanium oxide layer on the surface, which lowers the current. In stage II, the partial dissolution of titanium dioxide begins and the current subsequently rises to a maximum, as random pores appear in the initial compact oxide. In the last stage, the current attains a constant value or drops (stage III), as regular nanotube layers form. The penetrated compact oxide (initiation layer) often remains as a remnant that is frequently found after anodization on the tube tops [15,20,24]. Therefore, to provide better insight and precise interpretation of the results, the current density-time curves of the samples should be carefully investigated. Before that, it worth reviewing all the electrochemical reactions which occur in the electrochemical cell. The reactions which occur at the anode are as following [25]:

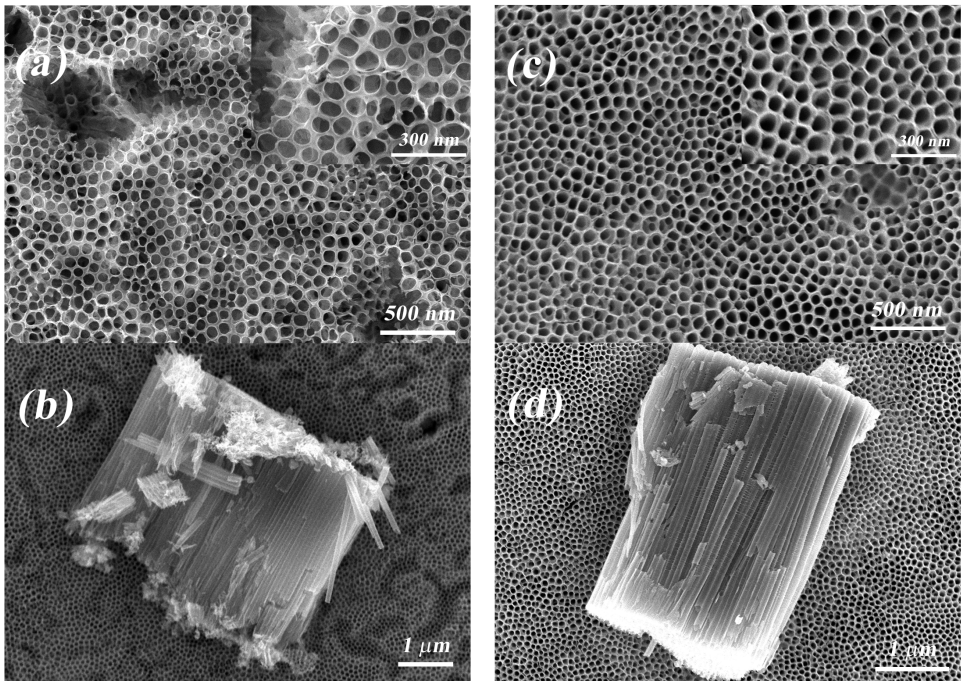

Fig. 3- FESEM images of surface morphology of (a) TNT-6, (b) TNT-2 and cross-section view of (c) TNT-6 and (d) TNT-2.

$$Ti \rightarrow Ti^{4+} + 4e^- \quad (2)$$
$$Ti^{4+} + 4OH^- \rightarrow Ti(OH)_4 \quad (3)$$
$$Ti^{4+} + 2O^{2-} \rightarrow TiO_2 \quad (4)$$
$$Ti(OH)_4 \rightarrow TiO_2 + 2H_2O \quad (5)$$

Oxidation of the metal which releases Ti^{4+} ions and electrons happens according to Eq. (2). Consequently, a combination of Ti^{4+} ions with OH^- and O^{2-} species are provided by the water components (Eq. (3) and (4)). Hydrated anodic layer releases water and further oxide is produced (Eq. (5)).

Hydrogen evolution takes place at the cathode side according to the following equation [25]:

$$8H^+ + 8e^- \rightarrow 4H_2 \quad (6)$$

Moreover, in the presence of fluoride ions some additional reactions may happen at the anode surface [25]:

$$TiO_2 + 6F^- + 4H^+ \rightarrow TiF_6^{2-} + H_2O \quad (7)$$
$$Ti(OH)_4 + 6F^- \rightarrow TiF_6^{2-} + 4OH^- \quad (8)$$
$$Ti^{4+} + 6F^- \rightarrow TiF_6^{2-} \quad (9)$$

The oxide layer and hydrated layer could be attacked by fluoride ions, as described in Eq. (7) and (8), and F^- can also react with Ti^{4+} according to Eq. (9). These equations describe the pores' initiation and growth. It is important to mention that during stage III, the initiation layer becomes thinner due to the chemical etching (Eqs. (7) to (9)) [15]. Based on the electrochemical reactions, the increased surface area of the cathode provides larger active sites. Thus, more H^+ ions should be generated due to enhanced hydrogen evolution reaction. The H^+ ions are produced through electrolysis of H_2O while OH^- ions are the other product of this reaction [26]. Therefore, more OH^- are also generated and hydration of Ti^{4+} which could be followed by oxidation of these species happens at a faster rate, Eqs. (3) and (5).

Fig. 4 illustrates the I-t curves of the synthesized samples. From Fig. 4a and b, it could be observed that a larger surface area of the cathode led to a significant increase in current density due to the increased reaction rate. Furthermore, stages I and II require less time to be completed. Higher current density at the course of the anodization can be observed during the plateau region (stage III). This balance is a result of the oxide formation and dissolution [20]. Therefore, according to Eqs. (7) to (9), the etching reaction becomes intensified and the initiation layer - as the most exposed part – and upper part of the tubes could be affected the most. Hence, the thinning of the initiation layer, followed by the integrity loss would be expected. Due to better access of electrolyte to the top part of the underneath TNTs, the further etching of the upper tube part weakens the structure which results in the collapse of the tubes wall on the TNTs. This kind of structure is known as nanograss, which introduces a detrimental impact on the performance of the TNTs. Nanograss structure can block the tube mouth and have a negative influence on the photocatalytic activity [14,15]. This phenomenon could be observed in Fig. 3a. As well as the increased current observed in Fig.

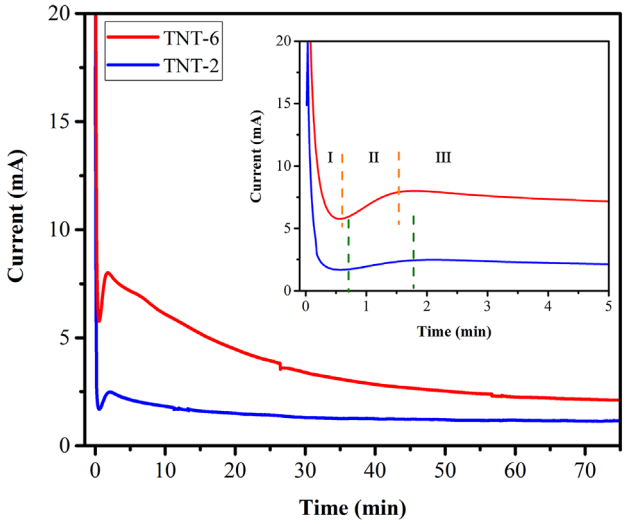

Fig. 4- Current density vs. time plots of the synthesized TNT.

4, longer tube length in TNT-6 compared to TNT-2 confirms the increased reaction rate during the anodization (Figs. 3c and d). Moreover, it has been demonstrated in our previous research [15] that the TNTs covered by the disordered initiation layer have a detrimental impact on their photocatalytic performance. The photocatalytic degradation of the sample covered by the disordered initiation layer decreased by 10% compared to TNTs covered by the ordered initiation layer [15]. Accordingly, to obtain an ordered structure and have a good control over the morphology of the synthesized TNTs, it is better to slow down the reaction during the anodization.

It has been previously concluded that the bandgap energy is unaffected by the surface morphology [15]. Therefore, the UV-vis absorption spectra was measured for TiO_2 nanotubes with ordered initiation layer (TNT-2) (Fig. 5). To calculate the bandgap energy of the synthesized TNTs (TNT-2), a plot of $(F(R)h\nu)^{0.5}$ vs. hν was calculated and presented in Fig. 5b. A good fit was obtained and according to the extrapolation a value of 3.22 eV was considered for the bandgap of TNT-2 sample. Hence, the corresponding bandgap wavelength was calculated to be 390 nm (Fig. 5a).

3.2 photocatalytic activity

Synthesizing TiO_2 in the form of nanotubes enhances the surface area significantly. These nanotubes offer enhanced reaction sites for photocatalytic degradation processes. Morphological features are well-documented to have a significant impact on the photocatalytic activities since the accessible surface area could be determined by tube-top morphology. Therefore, the photocatalytic activity of the TNT-2 sample with the ordered initiation layer was tested through photodegradation of MB under UV light irradiation. The following steps occur during the photocatalytic degradation processes [27]:

$$TiO_2 + h\nu \rightarrow TiO_2(e^-_{CB} + h^+_{VB}) \quad (10)$$

$$H_2O + h^+ \rightarrow OH\cdot + H^+ \quad (11)$$

$$O_2 + e^- \rightarrow O_2^- \quad (12)$$

According to Eq. 10, after the UV light irradiation ($h\nu \geq E_g = 3.2\ eV$), the photo-generated holes and electrons form in the valance and the conduction bands, respectively. These holes and electrons resulted in the oxidation of H_2O and the reduction of O_2, respectively (Eqs. 11 and 12) [27]. Oxidation of an organic pollutant via successive attacks by $OH\cdot$ radicals occur according to the following reaction:

$$R + OH\cdot \rightarrow R'\cdot + H_2O \quad (13)$$

where R is the organic pollutant. Direct oxidation by reaction with the holes is also possible:

$$R + h^+ \rightarrow R^{+\cdot} \quad (14)$$

In the case of MB, the $OH\cdot$ radicals attack and open the central aromatic rings of the organic compound via multistep intermediate reactions which result in the MB decomposition process [27,28]. The complete photo mineralization process by TiO_2 nanotubes or any other semiconductor photocatalyst is summarized by the following reaction [29]:

$$C_{16}H_{18}N_3SCl + 25\tfrac{1}{2}O_2 \rightarrow HCl + H_2SO_4 + 3HNO_3 + 16CO_2 + 6H_2O \quad (15)$$

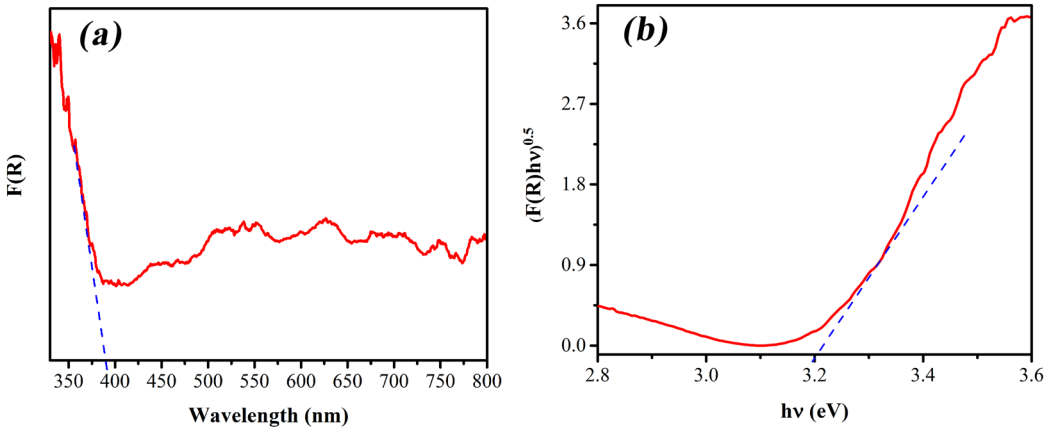

Fig. 5- UV-vis absorption spectra of TNT-2 sample (a) F(R) vs. wavelength, and (b) $(F(R)h\nu)^{0.5}$ vs. hν.

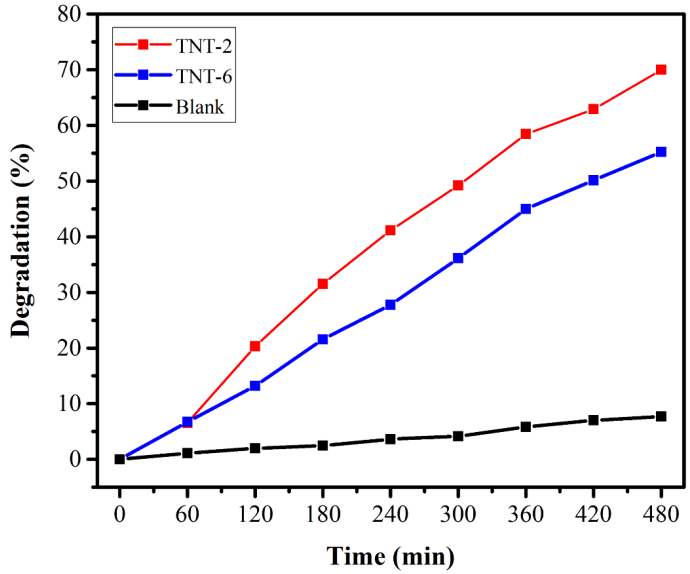

Fig. 6- The photocatalytic degradation of MB in the presence of TNTs array as photocatalyst.

Based on the reactions and the mechanism discussed above, the TiO_2 nanotubes act as a catalyst for the degradation of MB in the UV light irradiation. An ordered surface morphology provides better accessibility of the polluted water into the tubes while nanograss presence could block the entrance of the tubes [15]. Fig. 6 illustrates that after 480 min of photo irradiation, about 69% of MB was decomposed according to Eq. 15. Since for the TNT-6 sample which suffers from nanograss layer formation on the top of the NTs, this value was measured to be 58%.

4. Conclusions

The TiO_2 nanotubes (TNTs) were synthesized via a facile electrochemical anodization method. The effect of the surface area ratio of the cathode to the anode on the final surface morphology of the anodized samples was investigated. Considering the voltage and duration of the anodization process constant, it was concluded that the electrochemical reaction rate of the anodic processes was greatly affected by the surface area of the cathode. The smaller surface area ratio of the cathode to the anode (in sample TNT-2) made it possible to control the obtained structure with no damages on the surface morphology illustrating a better photocatalytic performance due to better accessibility of the polluted water into the tubes. After 480 min UV light irradiation and employing TNTs with ordered initiation layer as a photocatalyst, the photo-degradation of MB reached 69 %.

References

1. Lai Y, Sun L, Chen Y, Zhuang H, Lin C, Chin JW. Effects of the Structure of TiO2 Nanotube Array on Ti Substrate on Its Photocatalytic Activity. Journal of The Electrochemical Society. 2006;153(7):D123.
2. Daghrir R, Drogui P, Robert D. Modified TiO2For Environmental Photocatalytic Applications: A Review. Industrial & Engineering Chemistry Research. 2013;52(10):3581-99.
3. Paramasivam I, Jha H, Liu N, Schmuki P. A Review of Photocatalysis using Self-organized TiO2Nanotubes and Other Ordered Oxide Nanostructures. Small. 2012;8(20):3073-103.
4. Nah Y-C, Paramasivam I, Schmuki P. Doped TiO2 and TiO2 Nanotubes: Synthesis and Applications. ChemPhysChem. 2010;11(13):2698-713.
5. Moalej NS, Ahadi S, Sheibani S. Photocatalytic degradation of methylene blue by 2 wt.% Fe doped TiO2 nanopowder under visible light irradiation. Journal of Ultrafine Grained and Nanostructured Materials. 2019 Dec 1;52(2):133-41.
6. Shafei A, Sheibani S. Effect of hydrolysis rate on the properties of TiO2-CNT nanocomposite powder prepared by sol-gel method. Journal of Ultrafine Grained and Nanostructured Materials. 2018 Jun 1;51(1):90-5.
7. Ansari F, Sheibani S, Caudillo-Flores U, Fernández-García M. Effect of calcination process on the gas phase photodegradation by CuO-Cu2O/TiO2 nanocomposite photocatalyst. Journal of Ultrafine Grained and Nanostructured Materials. 2020 Jun 1;53(1):23-30.
8. Zhuang H-F, Lin C-J, Lai Y-K, Sun L, Li J. Some Critical Structure Factors of Titanium Oxide Nanotube Array in Its Photocatalytic Activity. Environmental Science & Technology. 2007;41(13):4735-40.
9. Chen Z, Fang L, Dong W, Zheng F, Shen M, Wang J. Inverse opal structured Ag/TiO2plasmonic photocatalyst prepared by pulsed current deposition and its enhanced visible light photocatalytic activity. J Mater Chem A. 2014;2(3):824-32.
10. Regonini D, Schmidt A, Aneziris CG, Graule T, Clemens FJ. Impact of the Anodizing Potential on the Electron Transport Properties of Nb-doped TiO2 Nanotubes. Electrochimica Acta. 2015;169:210-8.

11. Pang YL, Lim S, Ong HC, Chong WT. A critical review on the recent progress of synthesizing techniques and fabrication of TiO2-based nanotubes photocatalysts. Applied Catalysis A: General. 2014;481:127-42.
12. Huang C-y, Guo R-t, Pan W-g, Tang J-y, Zhou W-g, Liu X-y, et al. One-dimension TiO2 nanostructures with enhanced activity for CO2 photocatalytic reduction. Applied Surface Science. 2019;464:534-43.
13. Dikici T, Demirci S, Erol M. Enhanced photocatalytic activity of micro/nano textured TiO2 surfaces prepared by sandblasting/acid-etching/anodizing process. Journal of Alloys and Compounds. 2017;694:246-52.
14. Mazzarolo A, Lee K, Vicenzo A, Schmuki P. Anodic TiO2 nanotubes: Influence of top morphology on their photocatalytic performance. Electrochemistry communications. 2012 Aug 1;22:162-5.
15. Montakhab E, Rashchi F, Sheibani S. Modification and photocatalytic activity of open channel TiO2 nanotubes array synthesized by anodization process. Applied Surface Science. 2020;534:147581.
16. Cai Q, Paulose M, Varghese OK, Grimes CA. The Effect of Electrolyte Composition on the Fabrication of Self-Organized Titanium Oxide Nanotube Arrays by Anodic Oxidation. Journal of Materials Research. 2005;20(1):230-6.
17. Allam NK, Grimes CA. Effect of cathode material on the morphology and photoelectrochemical properties of vertically oriented TiO2 nanotube arrays. Solar Energy Materials and Solar Cells. 2008;92(11):1468-75.
18. López R, Gómez R, Llanos ME. Photophysical and photocatalytic properties of nanosized copper-doped titania sol–gel catalysts. Catalysis Today. 2009;148(1-2):103-8.
19. Regonini D, Jaroenworaluck A, Stevens R, Bowen CR. Effect of heat treatment on the properties and structure of TiO2 nanotubes: phase composition and chemical composition. Surface and Interface Analysis. 2010;42(3):139-44.
20. Regonini D, Bowen CR, Jaroenworaluck A, Stevens R. A review of growth mechanism, structure and crystallinity of anodized TiO2 nanotubes. Materials Science and Engineering: R: Reports. 2013;74(12):377-406.
21. Martin M, Leonid S, Tomáš R, Jan Š, Jaroslav K, Mariana K, et al. Anatase TiO 2 nanotube arrays and titania films on titanium mesh for photocatalytic NO X removal and water cleaning. Catalysis Today. 2017;287:59-64.
22. Eskandarloo H, Hashempour M, Vicenzo A, Franz S, Badiei A, Behnajady MA, et al. High-temperature stable anatase-type TiO2 nanotube arrays: A study of the structure–activity relationship. Applied Catalysis B: Environmental. 2016;185:119-32.
23. Ozkan S, Nguyen NT, Mazare A, Hahn R, Cerri I, Schmuki P. Fast growth of TiO 2 nanotube arrays with controlled tube spacing based on a self-ordering process at two different scales. Electrochemistry Communications. 2017;77:98-102.
24. Bonatto F, Venturini J, Frantz AC, dos Santos TCL, Bergmann CP, Brolo AG. One-step synthesis of nanograss-free TiO2 nanotubes using DTPA-enriched electrolytes. Ceramics International. 2018;44(18):22345-51.
25. Jaroenworaluck A, Regonini D, Bowen CR, Stevens R, Allsopp D. Macro, micro and nanostructure of TiO2 anodised films prepared in a fluorine-containing electrolyte. Journal of Materials Science. 2007;42(16):6729-34.
26. Li H, Chen Z, Tsang CK, Li Z, Ran X, Lee C, et al. Electrochemical doping of anatase TiO2in organic electrolytes for high-performance supercapacitors and photocatalysts. J Mater Chem A. 2014;2(1):229-36.
27. Sangpour P, Hashemi F, Moshfegh AZ. Photoenhanced Degradation of Methylene Blue on Cosputtered M:TiO2(M = Au, Ag, Cu) Nanocomposite Systems: A Comparative Study. The Journal of Physical Chemistry C. 2010;114(33):13955-61.
28. Houas A. Photocatalytic degradation pathway of methylene blue in water. Applied Catalysis B: Environmental. 2001;31(2):145-57.
29. Soltani T, Entezari MH. Photolysis and photocatalysis of methylene blue by ferrite bismuth nanoparticles under sunlight irradiation. Journal of Molecular Catalysis A: Chemical. 2013;377:197-203.